scientific reports

Check for updates

OPEN

Density functional theory study on the formation mechanism and electrical properties of two-dimensional electron gas in biaxial-strained $LaGaO_3/BaSnO_3$ heterostructure

Yuling Li[1], Yuxi Huang[1], Xiaohua Liu[1], Yaqin Wang[1,2]✉ & Le Yuan[1]

The two-dimensional electron gas (2DEG) in $BaSnO_3$-based heterostructure (HS) has received tremendous attention in the electronic applications because of its excellent electron migration characteristic. We modeled the *n*-type $(LaO)^+/(SnO_2)^0$ interface by depositing $LaGaO_3$ film on the $BaSnO_3$ substrate and explored strain effects on the critical thickness for forming 2DEG and electrical properties of $LaGaO_3/BaSnO_3$ HS system using first-principles electronic structure calculations. The results indicate that to form 2DEG in the unstrained $LaGaO_3/BaSnO_3$ HS system, a minimum thickness of approximately 4 unit cells of $LaGaO_3$ film is necessary. An increased film thickness of $LaGaO_3$ is required to form the 2DEG for -3%-biaxially-strained HS system and the critical thickness is 3 unit cells for 3%-baxially-strained HS system, which is caused by the strain-induced change of the electrostatic potential in $LaGaO_3$ film. In addition, the biaxial strain plays an important role in tailoring the electrical properties of 2DEG in $LaGaO_3/BaSnO_3$ HS syestem. The interfacial charge carrier density, electron mobility and electrical conductivity can be optimized when a moderate tensile strain is applied on the $BaSnO_3$ substrate in the *ab*-plane.

Recently, the two-dimensional electron gas (2DEG) at the *n*-type $(LaO)^+/(TiO_2)^0$ interface in $LaAlO_3/SrTiO_3$ heterostructures (HS) system has attracted considerable attention due to its unique interfacial properties and promising applications in the next-generation nanoelectronics[1–4]. The typical explanation for the formation of 2DEG is the so-called "polar catastrophe" mechanism[5,6]. The $LaAlO_3$ film is formed by alternating charged $(LaO)^+$ and $(AlO_2)^-$ layers, while the $SrTiO_3$ substrate is considered as stacks of neutral $(SrO)^0$ and $(TiO_2)^0$ layers. The *n*-type $(LaO)^+/(TiO_2)^0$ interface can be formed by growing $LaAlO_3$ films on the $SrTiO_3$ substrate. Then an electronic reconstruction occurs at the $LaAlO_3/SrTiO_3$ interface to compensate the polar discontinuity by migrating electrons from the interfacial polar $(LaO)^+$ layer to the adjacent non-polar $(TiO_2)^0$ layers.

Although the $LaAlO_3/SrTiO_3$ HS system exhibits a high interfacial carrier density with 3.2×10^{-14} cm^{-2}, the electron mobility is low (1 $cm^2V^{-1}s^{-1}$) at room temperature (RT), which limits its application in the photoelectric devices[7,8]. This phenomenon is originated from that the conduction band bottom of $SrTiO_3$ is composed of highly dispersed d_{xy} orbitals and the electrons on these orbitals show high mobility at low temperature. While it consists of lowly dispersed d_{xz}/d_{yz} orbitals at RT. The multi-band degeneracy leads to the inter-band transition scattering and stronger electron-phonon coupling effect, which reduces the electron mobility. To broaden the application of $LaAlO_3/SrTiO_3$ HS system at RT, some approaches are proposed to improve its interfacial electron mobility. For instance, defect engineering[9,10], strain engineering[11,12], and find other materials to replace the $SrTiO_3$ channel material[13,14]. Z. Q. Liu et al.[9] pesented that the interfacial carrier density of $LaAlO_3/SrTiO_3$ HS system at RT increases with the decrease of oxygen partial pressure, and the carrier mobility shows the opposite

[1]Key Laboratory of Fluid and Power Machinery, School of Material Science and Engineering, Xihua University, Chengdu 610039, People's Republic of China. [2]State Key Laboratory of Electronic Thin Films and Integrated Devices, University of Electronic Science and Technology of China, Chengdu 610054, People's Republic of China. ✉email: wangyqyyxf@sina.com

trend. Ariando et al.[12] reported that the electron mobility of interfacial 2DEG in $LaAlO_3/SrTiO_3$ HS system is sensitive to the biaxial strain. The biaxial compressive strain decreases the electron mobility and increases the interfaical carrier density. The largest electron mobility is $< 10\ cm^2V^{-1}s^{-1}$at RT. Zou et al.[13] prepared a polar/polar perovskite oxide heterostructure, that is, $LaTiO_3/KTaO_3$ HS system with $(LaO)^+/(TaO_2)^+$ interface, and found that this HS system exhibits high interfacial electron mobility of 21 $cm^2V^{-1}s^{-1}$ at RT, which is higher than that of well-known $LaAlO_3/SrTiO_3$ HS system. Therefore, the performance of $LaAlO_3/SrTiO_3$ HS system can be effectively regulated by perovskite channel material $KTaO_3$. The search for other channel materials with high electron mobility at RT to further improve the interfacial electron mobility of pervoskite-type HS system has become a research focus.

$BaSnO_3$ film with Sn 5*s* orbitals at the bottom of conduction bands has considered as an ideal material for oxide transistor channel material due to its high electron mobility at RT. This is because that the *s* orbitals are less localized than *d* orbitals, which results in larger band dispersion and lower electron effective mass. Compared with traditional $SrTiO_3$ films, $BaSnO_3$ film with *s* orbitals at the conduction band bottoms has extremely high electron mobility at RT, with a value of 150 $cm^2V^{-1}s^{-1}$[15]. Our group have explored the possibility of producing a high-mobility 2DEG in $LaGaO_3/BaSnO_3$ HS system using first-principles electronic structure calculations. This HS system presented twice larger electron mobility and enhanced interfacial conductivity compared to the prototype $LaAlO_3/SrTiO_3$ HS system[16]. Kookrin et al.[17] combined experimental and theoretical approach to study the different electrical properties of perovskite-type $LaInO_3/BaSnO_3$ HS system on MgO and $SrTiO_3$ substrates, which are well explained by the varying deep acceptor densities for the HS system on two different substrates. They also reported that when the thickness of $LaScO_3$ ($LaInO_3$) film is 12 unit cells, the interfacial charge density of HS system at RT is about $2.5 \times 10^{13}\ cm^{-2}$, and the electron mobility is about 20-25 $cm^2V^{-1}s^{-1}$, which is obviously higher than that of $LaAlO_3/SrTiO_3$ system. Moreover, with the increase of La concentration doped in $BaSnO_3$, the interfacial electron density and mobility of HS system shows an increasing trend[18,19]. Aggoune et al.[20] preliminally explored the formation mechanism of 2DEG and two-dimensional hole gas (2DHG) by regulating the polarity and thickness of $LaInO_3$ film, as well as the interface structure using the first-principles calculation. However, the detailed formation mechanism for 2DEG needs further systematically studied. Particularly, the changes of electrical properties of the $BaSnO_3$-based HS systems deposited on the substrates with different lattice parameters also need further investigation. This lattice mismatch between the HS system and substrate is easy to form growth strain, which is also usually induced by varying experimental preparation parameters and the uneven thermal diffusion during the heating/cooling process caused by the mismatch of thermal expansion coefficient between the HS system and substrate. Previous researchers[12,21] have found that this growth strain is generally in the range of – 3% ~ 3%. For example, Z. Huang et al.[12] selected four substrates with different lattice parameters to prepare Nb-$SrTiO_3$ thin film and $LaAlO_3/SrTiO_3$ HS system. The lattice mismatch between the HS system and substrate resulted in – 2.98% ($LaAlO_3$), – 0.96% (LSAT), 0 ($SrTiO_3$), and 0.99% ($DyScO_3$) strains, respectively. C. W. Bark et al.[21] deposited $LaAlO_3/SrTiO_3$ HS system on the substrates with different lattice parameters by pulsed laser deposition, resulting in a biaxial range of – 1.21% ($NdGaO_3$) ~ 1.59% ($GdScO_3$) in the HS system. Lan Meng et al.[22] prepared WS_2 film by chemical vapor deposition on SiO_2 /Si substrate, and then cooled it rapidly. In the process of rapidly cooling, the mismatch of thermal expansion coefficient between WS_2 film and substrate led to local stress in WS_2 film, but the stress/strain value was not referred to in this paper. Besides growth strain, we can dynamically regulate the force of film/heterostructure by artificially applying strain in the experiments, which is called "extrinsic strain". Then the range of strain can be artificially regulated according to the ultimate force of the material. For example, B Jalan et al.[23] applied different stresses on the epitaxial $SrTiO_3$ thin films by three-point bending, studying the changes of electron mobility of film with the temperature and stress.

In this work, we systematically investigated the $(LaGaO_3)_m/BaSnO_3$ HS models by means of the first-principles calculations. Firstly, the $LaGaO_3$ film thickness dependence of the formation of 2DEG in the unstrained $(LaGaO_3)_m/BaSnO_3$ HS model was studied. Next, we explored the influence of biaxial strain in the *ab*-plane on the critical thickness of $LaGaO_3$ film for forming 2DEG. The electrical properties of $LaGaO_3/BaSnO_3$ HS system dependent on the biaxial strain were analyzed from the electron effective mass, interfacial electron density, electron mobility, and electrical conductivity. This work may provide some guidances for adjusting the electrical properties of $LaGaO_3/BaSnO_3$ HS system by biaxial strain.

Results

Bulk parent compounds

First, we calculated the lattice parameters and energy band gap of $LaGaO_3$ and $BaSnO_3$ materials in their cubic phase, shown in Table S1 in the supporting information. The calculated lattice constants from GGA+U functional are well consistent with the experimental values (3.939 vs 3.860 Åfor $LaGaO_3$ and 4.186 vs 4.115 Åfor $BaSnO_3$)[24,25]. In contrast, the calculated energy band gaps from the GGA+U approach are underestimated with respect to the experimental values (3.668 vs 4.4 eV for $LaGaO_3$ and 2.208 vs 3.1 eV for $BaSnO_3$)[26,27], which is due to the well-known shortcoming of the GGA functional that cannot give an accurate description for the electron-electron correlation-exchange interaction. However, this underestimation has been determined that it has no influence on our conclusions about the 2DEG at the perovskite-type HS systems because the electronic states that contribute to the formation of DEG can be well reproduced from GGA+U calculations[28–30]. Then our GGA+U approach can well predict the 2DEG-related Sn 5*s* states as well as the critical thickness of the $LaGaO_3$ for forming the 2DEG in the $LaGaO_3/BaSnO_3$ HS system.

2DEG in the *n*-type $LaGaO_3/BaSnO_3$ HS system

The calculated total density of states (DOS) for the *n*-type $(LaGaO_3)_m/BaSnO_3$ HS system with different $LaGaO_3$ unit cells (*m*=2, 3, 4, 5, 6 and 8) are shown in Fig. 1, where the vertical dotted line at 0 eV represents the fermi level. At m=2 and 3, the fermi level of $(LaGaO_3)_m/BaSnO_3$ HS system is on the top of the valence bands, and the HS system shows insulating characteristics. The band gap of HS system decreases with the increase of $LaGaO_3$ film thickness. While at m=4, 5, 6 and 8, the band gap disappears and all the HS models exhibit metallic properties. With the increase of $LaGaO_3$ film thickness, the metallic states near the fermi level increase. These results indicate that the critical thickness of insulator-to-metal transition is 4 unit cells for $LaGaO_3$ film in the *n*-type $LaGaO_3/BaSnO_3$ HS system, which is similar to the case of well-known *n*-type $LaAlO_3/SrTiO_3$ HS model[31].

To further understand the origin and charge transfer of metallic electronic states in the *n*-type $(LaGaO_3)_m/BaSnO_3$ HS system, We calculated the layer-resolved partial DOS for *n*-type $(LaGaO_3)_m/BaSnO_3$ HS system at m=2, 4 and 8, as shown in Figs. 2, S1 in the supporting information and Fig. 3, respectively. To directly observe the contribution of each layer to the metallic states, we calculated the charge density projected on metallic bands for each model. For the convenience of discussion, the first and second layers of SnO_2 are defined as IF-I and IF-II, respectively. For the $(LaGaO_3)_2/BaSnO_3$ HS system in Fig. 2, the layer-resolved partial DOS and the charge density show that the fermi level does not cross the conduction bands and valence bands. Then there are no metallic states exist in the IF-I and IF-II layers, and the HS system shows insulating characteristic. These phenomena can be clearly seen in the enlarged view of IF-I and IF-II layers in Fig. 2b. Since the polarization strength of $LaGaO_3$ film in $(LaGaO_3)_2/BaSnO_3$ HS system is strong enough to make the electrons transfer from the $(LaO)^+$ layer to $(GaO_2)^-$ layer, neutralizing the holes in $(GaO_2)^-$ layer. Then there exist no holes on the surface and no electrons at the interface. The polar discontinuity in the *n*-type $(LaO)^+/(SnO_2)^0$ interface is offset by strong polarization in $LaGaO_3$ film, which is similar to the $LaAlO_3/SrTiO_3$ HS system[31].

For the $(LaGaO_3)_8/BaSnO_3$ HS system in Fig. 3, the fermi level passes through the valence bands of the surface $(GaO_2)^-$ layer, showing *p*-type conducting states. While the interface indicates *n*-type conducting states from the interfacial $(SnO_2)^0$ layer. Then the overlap of these states make the $(LaGaO_3)_8/BaSnO_3$ HS system show metallic property in Fig. 1. The O2*p* states of $(LaO)^+$ and $(GaO_2)^-$ layers significantly shift toward higher energy with the layers move from the interfacial $(LaO)^+$ layer to the surface $(GaO_2)^-$layer, presenting the electrostatic potential in the $LaGaO_3$ film. This is because that the $LaGaO_3$ film in the $(LaGaO_3)_8/BaSnO_3$ HS model exhibits a weaker polarization than that in the $(LaGaO_3)_2/BaSnO_3$ HS model, which is not enough to offset the polarity discontinuity between $LaGaO_3$ and $BaSnO_3$. Thus, there exist *p*-type conducting states from O 2*p* orbitals on the $LaGaO_3$ surface. In short, the $(LaGaO_3)_8/BaSnO_3$ HS system present metallic properties with the *p*-type conducting states from O 2*p* orbitals on the surface and the *n*-type conducting states from Sn 5*s* orbitals at the interface.

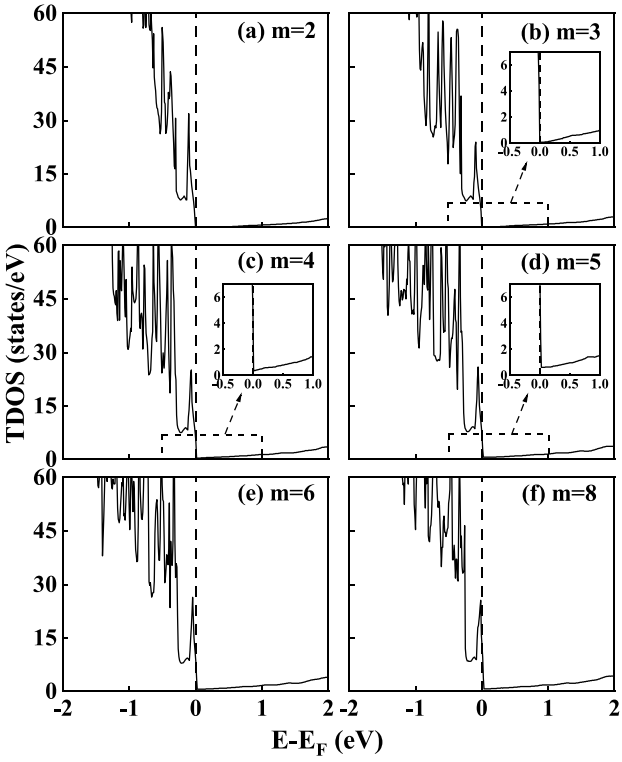

Figure 1. Calculated total density of states (DOS) for the *n*-type $(LaGaO_3)_m/BaSnO_3$ HS models with different $LaGaO_3$ unit cells. (**a**) m = 2, (**b**) m = 3, (**c**) m = 4, (**d**) m = 5, (**e**) m = 6 and (**f**) m = 8. The vertical dashed line indicates the Fermi level at 0 eV in this and each subsequent DOS plot. The insets are the enlarged view of the DOS near fermi level for models.

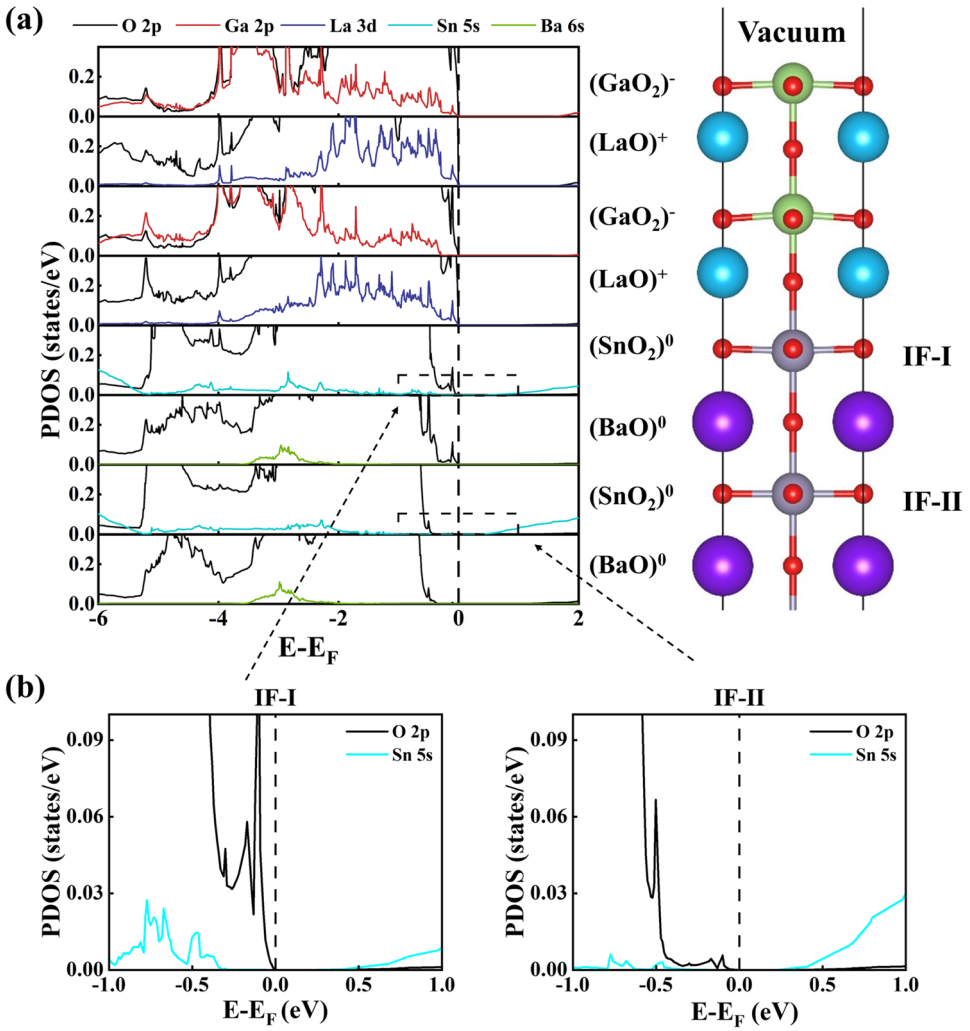

Figure 2. Calculated layer-resolved partial DOS for the *n*-type $(LaGaO_3)_2/BaSnO_3$ HS model along with the charge density projected on bands forming the 2DEG.

To clearly present the transition from the insulating characteristic to the metallic property of $LaGaO_3/BaSnO_3$ HS system, we also calculated the layer-resolved partial DOS for the *n*-type $(LaGaO_3)_4/BaSnO_3$ HS model along with the charge density projected on bands forming the 2DEG, shown in Fig. S1 in the supporting information. All the characteristics of $(LaGaO_3)_4/BaSnO_3$ HS model are consistent with that of $(LaGaO_3)_8/BaSnO_3$ HS system, except that the surface and interface metallic states are less. To quantify the change of interfacial electron concentration of the $(LaGaO_3)_m/BaSnO_3$ HS system with the $LaGaO_3$ film thickness, we also calculated their interfacial electron concentration by integrating the partial DOS of the Sn 5*s* orbitals near the fermi level from the interfacial IF-I and IF-II $(SnO_2)^0$ layer divided by the interfacial area, shown in Fig. 4a. As a comparison, the interfacial carrier concentration of $(LaAlO_3)_m/SrTiO_3$ HS system are also calculated in Fig. 4a, which is about $2–6\times10^{13}$ cm^{-2} at $m \geq 5$. For $(LaGaO_3)_m/BaSnO_3$ HS system, at $m \leq 3$, the interfacial electron concentration is zero; at $m \geq 4$, as m increases, the interfacial electron concentration increases. Similar to $LaAlO_3/SrTiO_3$ HS system, a sudden increase of interfacial electron concentration in $LaGaO_3/BaSnO_3$ HS system occur from m=4 to m=5. But he values of electron concentration are on the order of 10^{12} cm^{-3}, which is about an order of magnitude smaller than that in the corresponding $(LaAlO_3)_m/SrTiO_3$ HS system. This is because that the Sn 5*s* orbitals are more dispersive and poorly localized for electrons than the Ti 3*d* orbitals. This phenomenon is unfavorable to the practical application of 2DEG. Therefore, we indicate that the localization of interfacial electrons for the $BaSnO_3$-based HS system can be improved by doping the elements who have *d* orbitals. This method has already been used to modify the electrical properties of $BaSnO_3$ film. For example, Bing Li *etal.*[32] prepared Nb doped $BaSnO_3$ films by pulsed laser deposition, showing that the $BaNb_{0.05}Sn_{0.95}O_3$ film simultaneously has a high electron mobility of 19.65 $cm^2V^{-1}s^{-1}$and electron density of 6.59×10^{20} cm^{-3}, which is beneficial to its application in optoelectronic devices.

To analyze the change of interfacial 2DEG for $LaGaO_3/BaSnO_3$ HS system with different $LaGaO_3$ film thickness, the average polarization strength in the $LaGaO_3$ film was calculated by the following equation[33,34]:

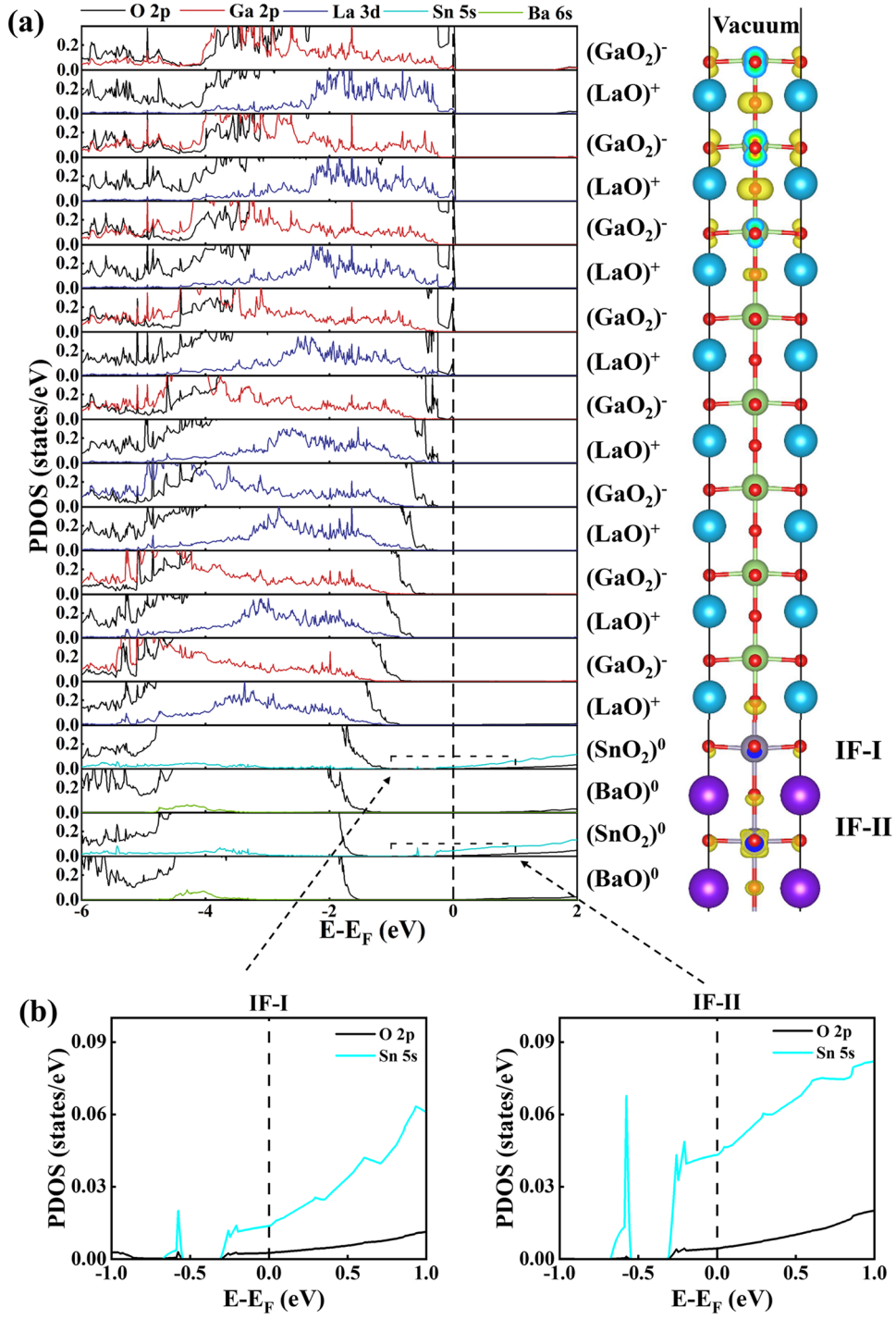

Figure 3. Calculated layer-resolved partial DOS for the *n*-type $(LaGaO_3)_8/BaSnO_3$ HS model along with the charge density projected on bands forming the 2DEG. The isovalue of 1.1×10^{-4} e/bohr^3 is used to produce the charge density plots.

$$P = \frac{e}{\Omega}\sum_{i=1}^{N} Z_i^* \cdot \delta_{z_i} \tag{1}$$

where Ω is the total volume of the $LaGaO_3$ film, N is the total number of atoms in the unit cell, Z_i^* is the Born effective charge of each atom, and δ_{z_i} is the relative displacement of the ith atom in the HS system. The relative displacement δ_{z_i} of La(Ga) atoms with respect to the oxygen atom in the same LaO and GaO_2 layers is calculated as $\delta_{z_{La/Ga}} = z_{La/Ga} - z_O$. Our calculated Born effective charge Z_i^* for La and Ga atoms are 4.03 and 3.34, respectively.

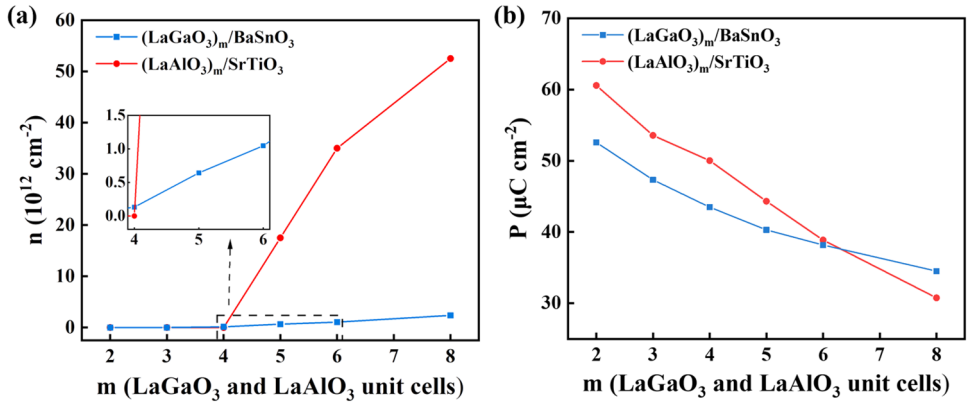

Figure 4. (**a**) Calculated interfacial charge carrier density (*n*) and (**b**) Polarization strength (P) in $LaGaO_3$ ($LaAlO_3$) film for the *n*-type $LaGaO_3/BaSnO_3$ ($LaAlO_3/SrTiO_3$) HS system as a function of $LaGaO_3$ ($LaAlO_3$) unit cells. The inset is the locally enlarged view of interfacial charge carrier density for $LaGaO_3/BaSnO_3$ HS system.

The calculated polarization strength in the $LaGaO_3$ film of *n*-type $(LaGaO_3)_m/BaSnO_3$ HS system with different $LaGaO_3$ thickness are shown in Fig. 4b. As the $LaGaO_3$ film thickness increases from 2 to 8, the average polarization strength in the $LaGaO_3$ film decreases from 52.59 $\mu C \cdot cm^{-2}$ to 34.52 $\mu C \cdot cm^{-2}$, indicating that the electrostatic force drives the electron from $(LaO)^+$ layer to $(GaO_2)^-$ layer is weaken, leading to the increase of interfacial electron density. Combined with the total DOS diagram in Fig. 1, it can be concluded that the critical polarization strength of insulator-to-metal transition for $LaGaO_3/BaSnO_3$ HS system is 43.50 $\mu C \cdot cm^{-2}$ (polarization strength at m=4), which is lower than that of $LaAlO_3/SrTiO_3$ HS system with the value of 50.03 $\mu C \cdot cm^{-2}$.

2DEG in the strained $LaGaO_3/BaSnO_3$ HS system

Based on the discussions above, we know that the critical thickness of insulator-to-metal transition for the unstrained $(LaGaO_3)_m/BaSnO_3$ HS system is 4 unit cells. The formation of 2DEG at the interface is strongly related to the distortion of $LaGaO_3$ film. To study the changes of interfacial electronic states induced by this distortion, we calculated the total DOS of $(LaGaO_3)_m/BaSnO_3$ (m=2, 3, 4, and 5) HS models with different biaxial strains of −3%, −2%, 2%, and 3%, as shown in Fig. 5. The "+" and "−" signs indicate tensile and compressive strains, respectively. Our calculated total DOS shows that all the $(LaGaO_3)_2/BaSnO_3$ HS models with − 3%, − 2%, 0, 2%, and 3% strains show semiconducting characteristics (first row in Fig. 5). While the $(LaGaO_3)_3/BaSnO_3$ HS model with − 3%, − 2%, and 0 strains and the $(LaGaO_3)_4/BaSnO_3$ HS model with −3% strain also show a similar semiconducting behavior. With the strain from −3% to 3%, the band gap of $(LaGaO_3)_4/BaSnO_3$ HS model decreases and vanishes. A small number of states present at the fermi level for the models with 0, 2% and 3% strains, thus exhibiting weak metallicity. All the $(LaGaO_3)_5/BaSnO_3$ HS models exhibit metallic properties and more states arise near the fermi level with the strain from compressive to tensile. In short, we can obtain the following conclusions: (1) For the unstrained $(LaGaO_3)_5/BaSnO_3$ HS system, 4 unit cells of $LaGaO_3$ is the minimum critical thickness to obtain a 2DEG; (2) For the −3%-biaxially-strained HS system, a critical thickness of 5 unit cells of $LaGaO_3$ is required, while 3 unit cells are the minimum requirement to form a 2DEG for the 3%-biaxially-strained HS system. These results present biaxial strains on the $BaSnO_3$ substrate has a significant impact on the critical thickness of $LaGaO_3$ film for forming 2DEG.

To exhibit the distribution of 2DEG for the *n*-type $(LaGaO_3)_m/BaSnO_3$ HS models with various biaxial strains, we further plotted the partial density states of Sn 5*s* orbitals in IF-I and IF-II layers for $(LaGaO_3)_4/BaSnO_3$ HS system with the biaxial strains of − 3%, 0, and 3% in Fig. S2 in the supporting information. The fermi level of the $(LaGaO_3)_4/BaSnO_3$ HS system with −3% strain does not cross the Sn 5*s* orbitals, exhibiting an insulating property. But for the unstrained and 3%-strained $(LaGaO_3)_4/BaSnO_3$ HS models, the fermi level crosses the Sn 5*s* orbitals, showing an metallic property. Moreover, the 3%-strained $(LaGaO_3)_4/BaSnO_3$ HS system has a higher concentration of electronic states near the fermi level compared to the unstrained HS system.

To further understand the change of electronic states at the interface, the polarization strength of $(LaGaO_3)_4/BaSnO_3$ HS system with the biaxial strain from − 3 to 3% is calculated, as shown in Fig. 6. The average polarization strength of $(LaGaO_3)_4/BaSnO_3$ HS system decreases with the biaxial strains from − 3 to 3%. In Fig. 4, we know that the critical polarization strength of unstrained $LaGaO_3/BaSnO_3$ HS system is 43.50 $\mu C \cdot cm^{-2}$ corresponding to the values of HS system with 4-unit-cells thickness of $LaGaO_3$ film. The average polarization strength of compressively-strained $(LaGaO_3)_4/BaSnO_3$ HS system is larger than that of the unstrained HS system. The electrostatic force prevent electron transfer from $(LaO)^+$ layer to $(GaO_2)^-$ layer is strengthen, resulting in insulating behavior for the compressively-strained $(LaGaO_3)_4/BaSnO_3$ HS system. On the opposite, the average polarization strength of tensilely-strained HS system is smaller than that of the unstrained HS system. Then the electrostatic force present the electron from $(LaO)^+$ layer to $(GaO_2)^-$ layer is weaken, thus the $(LaGaO_3)_4/BaSnO_3$ HS system under biaxial tensile strain present a metallic property. Overall, the polarization strength of $(LaGaO_3)_4/BaSnO_3$ HS system is strongly influenced by the biaxial strain, which determining the critical thickness of insulator-to-metal transition.

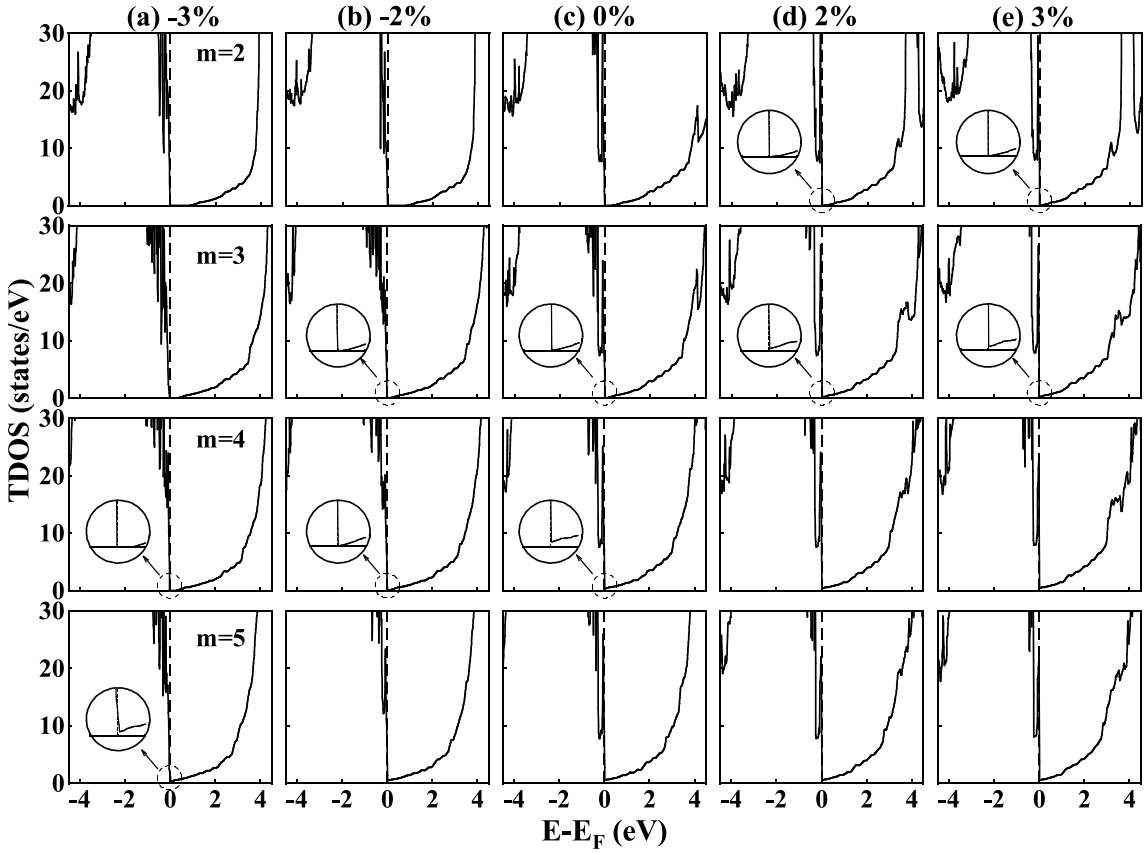

Figure 5. Calculated total DOS for the *n*-type $(LaGaO_3)_m/BaSnO_3$ (m =2, 3, 4, and 5) HS models with different strains. (**a**) − 3%, (**b**) − 2%, (**c**) 0%, (**d**) 2% and (**e**) 3%. The insets are the enlarged view of the DOS near fermi level for models.

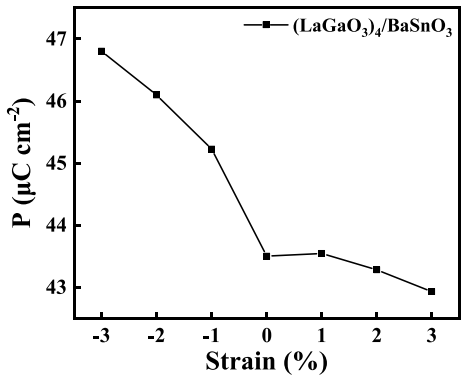

Figure 6. Calculated average polarization strength (P) in the $LaGaO_3$ film for *n*-type $(LaGaO_3)_4/BaSnO_3$ HS models with different biaxial strains.

Next, we calculated the electronic band structures for the strained $(LaGaO_3)_4/BaSnO_3$ HS system along the path M-Γ-X of the interfacial Brillouin zone compared to the unstrained model, shown in Fig. S3 in the supporting information. Some electronic states reside below the fermi level for the unstrained and tensilely-strained $(LaGaO_3)_4/BaSnO_3$ HS system, indicating metallic properties. While the compressively-strained HS system exhibit an insulating property. Further, we calculated the electron effective mass (m^*/m_0) for the minimum conduction bands along the Γ-*X* and Γ-*M* directions, in which m_0 is the electron effective mass for free electron. The electron effective mass m* was calculated using the parabolic approximation by the following formula[35]:

$$\frac{1}{m^*} = \frac{1}{\hbar^2}\frac{\partial^2 E_{CB}}{\partial \kappa^2} \tag{2}$$

where $\hbar$ is the reduced plank constant, κ is the corresponding wave vector of the conduction bands, and E_{CB} is the energy of the minimum conduction band. For the unstrained $(LaGaO_3)_4/BaSnO_3$ HS system, the calculated electron effective mass is $0.24m_0$, which is in good agreement with that of $BaSnO_3$ bulk[36]. As the biaxial strain changes from −3% to 3%, the electron effective mass decreases from $0.27m_0$ to $0.18m_0$. That is, the biaxial compressive strains harm the electron migration characteristic, and the tensile strains play the opposite role. What's more, we calculated the charge carrier density by integrating the layer-resolved partial DOSs for the conducting states below the fermi level from the interfacial IF-I and IF-II $(SnO_2)^0$ layer, see Fig. 7a. The HS systems with biaxial strains from −3 to 3% exhibit an increasing charge density from 0 to $4.49\times10^{12}cm^{-2}$, which provides evidence that the biaxial compressive strain suppresses the production of 2DEG, and the biaxial tensile strain promotes the formation of 2DEG at the interface.

Besides the interfacial charge density, the electron mobility is also an important factor in determining the interfacial conductivity of the 2DEG. We calculated the normalized electron mobility (μ/μ_0) and normalized electrical conductivity (σ/σ_0) for $(LaGaO_3)_4/BaSnO_3$ HS system under different biaxial strains, see Fig. 7b. μ_0 and σ_0 refer to the electron mobility and electrical conductivity of the unstrained $(LaGaO_3)_4/BaSnO_3$ HS system, respectively. The following two Eqs. (3) and (4) were used[37]:

$$\mu = e < \tau > /m^* \tag{3}$$

$$\sigma = ne\mu \tag{4}$$

where e, $< \tau >$, m^* , n, μ, and σ are the elementary charge, average scattering time, electron effective mass, interfacial electron density, electron mobility, and electrical conductivity, respectively. The scattering time τ is determined by all the scattering events, i.e. impurity scattering, electron-phonon scattering and electron-electron scattering. The inverse of τ can be described as the sum of rates associated with all the scattering mechanisms according to Matthiessen's rule[38]. It has been extremely challenging to calculate the scattering time τ due to the complicated scattering mechanisms. One common and simplified approach is to treat τ as a constant, which has been validated in prior studies[35,39,40] and used in this work. The electron mobility and the electrical conductivity of $(LaGaO_3)_4/BaSnO_3$ HS system with different biaxial strains are presented in Fig. 7b. As the biaxial strain changes from −3 to 3%, the value of μ/μ_0 and σ/σ_0 increases. Compared to the unstrained HS system, the μ/μ_0 and σ/σ_0 for compressively-strained $(LaGaO_3)_4/BaSnO_3$ HS system show lower, while for tensilely-strained HS system present higher.

Discussion

In conclusion, the insulator-to-metal transition critical thickness and electrical properties of unstrained and strained $LaGaO_3/BaSnO_3$ HS slab systems are studied using density functional theory calculations. The results show that a critical thickness of 4 unit cells for $LaGaO_3$ film is required for forming 2DEG in the unstrained $LaGaO_3/BaSnO_3$ HS system, while the critical thickness of $LaGaO_3$ film increases up to 5 unit cells in – 3%-biaxially-strained HS system and decreases to 3 unit cells in 3%-biaxially-strained HS system. These results are originated from that the biaxial strain along *ab* plane on the $BaSnO_3$ substrate can significantly affects the polarization strength in the $LaGaO_3$ film. We also find that the biaxial tensile strain can considerably increase the interfacial charge carrier density, electron mobility and electrical conductivity, while the biaxial compressive strain shows the opposite effect. In short, the interfacial electrical properties of 2DEG in $LaGaO_3/BaSnO_3$ HS system can be optimized by applying a tensile strain on the $BaSnO_3$ substrate along the *ab*-plane.

Methods

In this work, all the density functional theory (DFT)[41] calculations were carried out using the Vienna Ab initio Simulation Package (VASP)[42,43]. The projector augmented-wave (PAW) potentials were applied for electron-ion interactions[44]. The generalized gradient approximation (GGA) parameterized by Perdew-Burke-Ernzerhof (PBE) with the on-site Coulomb interaction approach (GGA+U) was employed for the exchange-correlation

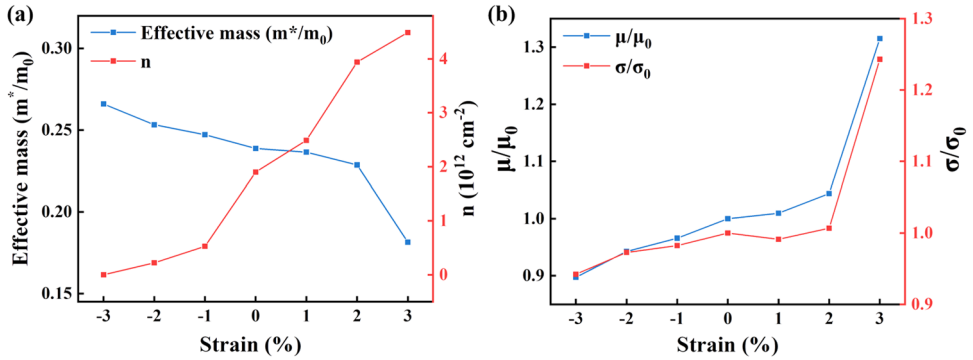

Figure 7. (**a**) The electron effective mass (m^*/m_0) and interfacial electron density (n), (**b**) The normalized electron mobility (μ/μ_0) and normalized electrical conductivity (σ/σ_0) for the $(LaGaO_3)_4/BaSnO_3$ HS model under different biaxial strains.

functional[45]. Since the electronic properties of perovskite oxides are sensitive to the U value of transition metal ions. An empirical U value of 7.5 eV was used to describe La 4*f* orbitals. A cutoff energy of 450 eV was used for the plane-wave basis set, and k-space grids of 10×10×1 within the monkhorst-pack scheme[46] were employed to converge the total energy. The electronic self-consistency calculation was assumed for a total energy convergence of less than 10^{-5} eV. All the atomic position were optimized until the interatomic forces smaller than 0.03 eV $Å^{-1}$.

$BaSnO_3$ crystallizes in a cubic phase with a space number of 211 ($Pm\bar{3}m$) at RT[47], while $LaGaO_3$ exhibits an orthogonal perovskite structure. A symmetric sandwich-type structural model, $(LaGaO_3)_m/(BaSnO_3)_{12.5}/(LaGaO_3)_m$, was built to model the *n*-type $(LaO)^+/(SnO_2)^0$ interface by adding different thickness of $LaGaO_3$ film on the SnO_2-terminated $BaSnO_3$ with the thickness of 12.5 unit cells. A vacuum layer of 20 Å was added on the GaO_2-terminated $LaGaO_3$ films to avoid the dipole-dipole interaction between the periodic slabs. To model the epitaxial growth process, all the ions were fully relaxed with fixed lattice parameters along the *ab* plane. The value of *m* was set from 2 to 8 to figure out the formation mechanism of 2DEG at the interface. The lattice parameter was changed to simulate various strains from − 3 to 3%, at intervals of 1% in the *ab* plane.

Data availability

The data that support the findings of this study are not openly available, but are available from the corresponding author upon reasonable request. If necessary, please contact the corresponding author: wangyqyyxf@sina.com.

Received: 3 February 2024; Accepted: 29 April 2024
Published online: 04 May 2024

References

1. Ohtomo, A. & Hwang, H. A high-mobility electron gas at the $LaAlO_3/SrTiO_3$ heterointerface. *Nature* **427**, 423–426. https://doi.org/10.1038/nature02308 (2004).
2. Cen, C. *et al.* Nanoscale control of an interfacial metal-insulator transition at room temperature. *Nat. Mater.* **7**, 298–302. https://doi.org/10.1038/nmat2136 (2008).
3. Cen, C., Thiel, S., Mannhart, J. & Levy, J. Oxide nanoelectronics on demand. *Science* **323**, 1026–1030. https://doi.org/10.1126/science.1168294 (2009).
4. Stornaiuolo, D. *et al.* Weak localization and spin-orbit interaction in side-gate field effect devices at the $LaAlO_3/SrTiO_3$ interface. *Phys. Rev. B* **90**, 235426. https://doi.org/10.1103/PhysRevB.90.235426 (2014).
5. Savoia, A., Paparo, D., Perna, P., Ristic, Z. & Marrucci, L. Polar catastrophe and electronic reconstructions at the $LaAlO_3/SrTiO_3$ interface: Evidence from optical second harmonic generation. *Phys. Rev. B*https://doi.org/10.1103/PhysRevB.80.075110 *(2009)*.
6. Nanda, B. R. K. & Satpathy, S. Polar catastrophe, electron leakage, and magnetic ordering at the $LaMnO_3/SrMnO_3$ interface. *Phys. Rev. B*https://doi.org/10.1103/PHYSREVB.81.224408 *(2010)*.
7. Förg, B., Richter, C. & Mannhart, J. Field-effect devices utilizing $LaAlO_3$-$SrTiO_3$ interfaces. *Appl. Phys. Lett.* **100**, 053506. https://doi.org/10.1063/1.3682102 (2012).
8. Irvin, P. *et al.* Anomalous high mobility in $LaAlO_3/SrTiO_3$ nanowires. *Nano Letters* **13**, 364–368. https://doi.org/10.1021/nl3033729 (2013).
9. Liu, Z. *et al.* Origin of the two-dimensional electron gas at $LaAlO_3/SrTiO_3$ interfaces: The role of oxygen vacancies and electronic reconstruction. *Phys. Rev. X* **3**, 021010. https://doi.org/10.1103/PhysRevX.3.021010 (2013).
10. Weston, L., Cui, X., Ringer, S. & Stampfl, C. Density-functional prediction of a surface magnetic phase in $SrTiO_3/LaAlO_3$ heterostructures induced by al vacancies. *Phys. Rev. Lett.* **113**, 186401. https://doi.org/10.1103/PhysRevLett.113.186401 (2014).
11. Kalisky, B. *et al.* Locally enhanced conductivity due to the tetragonal domain structure in $LaAlO_3/SrTiO_3$ heterointerfaces. *Nat. Mater.* **12**, 1091–1095. https://doi.org/10.1038/NMAT3753 (2013).
12. Huang, Z. *et al.* Biaxial strain-induced transport property changes in atomically tailored $SrTiO_3$-based systems. *Phys. Rev. B* **90**, 125156. https://doi.org/10.1103/PhysRevB.90.125156 (2014).
13. Zou, K. *et al.* $LaTiO_3/KTaO_3$ interfaces: A new two-dimensional electron gas system. *APL Mater.* **3**, 036104. https://doi.org/10.1063/1.4914310 (2015).
14. Wang, Y., Tang, W., Cheng, J., Behtash, M. & Yang, K. Creating two-dimensional electron gas in polar/polar perovskite oxide heterostructures: First-principles characterization of $LaAlO_3/A^+B^{5+}O_3$. *ACS Appl. Mater. Interfaces* **8**, 13659–13668. https://doi.org/10.1021/acsami.6b02399 (2016).
15. Raghavan, S. *et al.* High-mobility $BaSnO_3$ grown by oxide molecular beam epitaxy. *APL Mater.* **4**, 016106. https://doi.org/10.1063/1.4939657 (2016).
16. Wang, Y., Tang, W., Cheng, J., Nazir, S. & Yang, K. High-mobility two-dimensional electron gas in $SrGeO_3$-and $BaSnO_3$-based perovskite oxide heterostructures: An ab initio study. *Phys. Chem. Chem. Phys.* **18**, 31924–31929. https://doi.org/10.1039/C6CP05572A (2016).
17. Kim, Y. M. *et al.* Interface polarization model for a 2-dimensional electron gas at the $BaSnO_3/LaInO_3$ interface. *Sci. Rep.* **9**, 16202. https://doi.org/10.1038/s41598-019-52772-8 (2019).
18. Cho, H., Song, D., Kim, Y., Kim, B. & Char, K. High-mobility field-effect transistor using 2-dimensional electron gas at the $LaScO_3$ /$BaSnO_3$ interface. *ACS Appl. Electron. Mater.* **4**, 356–366. https://doi.org/10.1021/acsaelm.1c01048 (2022).
19. Kim, Y. M., Kim, Y. & Char, K. The role of coherent epitaxy in forming a two-dimensional electron gas at $LaIn_{1-x}Ga_xO_3/BaSnO_3$ interfaces. *Commun. Mater.* **2**, 73. https://doi.org/10.1038/s43246-021-00179-2 (2021).
20. Aggoune, W. & Draxl, C. Tuning two-dimensional electron and hole gases at $LaInO_3/BaSnO_3$ interfaces by polar distortions, termination, and thickness. *NPJ Comput. Mater.* **7**, 174. https://doi.org/10.1038/s41524-021-00646-x (2021).
21. Bark, C. W. *et al.* Tailoring a two-dimensional electron gas at the $LaAlO_3/SrTiO_3$ (001) interface by epitaxial strain. *Proc. Natl. Acad. Sci.* **108**, 4720–4724. https://doi.org/10.1073/pnas.1014849108 (2011).
22. Meng, L. *et al.* Two dimensional WS_2 lateral heterojunctions by strain modulation. *Appl. Phys. Lett.* **108**, 263104. https://doi.org/10.1063/1.4954991 (2016).
23. Jalan, B., Allen, S. J., Beltz, G. E., Moetakef, P. & Stemmer, S. Enhancing the electron mobility of $SrTiO_3$ with strain. *Appl. Phys. Lett.* **98**, 132102. https://doi.org/10.1063/1.3571447 (2011).
24. Perna, P. *et al.* Conducting interfaces between band insulating oxides: The $LaGaO_3/SrTiO_3$ heterostructure. *Appl. Phys. Lett.* **97**, 152111. https://doi.org/10.1063/1.3496440 (2010).
25. Ogisu, K. *et al.* Electronic band structures and photochemical properties of La-Ga-based oxysulfides. *J. Phys. Chem. C* **112**, 11978–11984. https://doi.org/10.1021/jp802153t (2008).
26. Zhang, W., Tang, J. & Ye, J. Structural, photocatalytic, and photophysical properties of perovskite $MSnO_3$ (M = Ca, Sr, and Ba) photocatalysts. *J. Mater. Res.* **22**, 1859–1871. https://doi.org/10.1557/jmr.2007.0259 (2007).

27. Wadekar, P. V. *et al.* Improved electrical mobility in highly epitaxial la: $BaSnO_3$ films on $SmScO_3$ (110) substrates. *Appl. Phys. Lett.* **105**, 052104. https://doi.org/10.1063/1.4891816 (2014).
28. Nazir, S., Cheng, J. & Yang, K. Creating two-dimensional electron gas in nonpolar/nonpolar oxide interface via polarization discontinuity: First-principles analysis of $CaZrO_3/SrTiO_3$ heterostructure. *ACS Appl. Mater. Interfaces* **8**, 390–399. https://doi.org/10.1021/acsami.5b09107 (2016).
29. Nazir, S. & Yang, K. First-principles characterization of the critical thickness for forming metallic states in strained $LaAlO_3/SrTiO_3$ (001) heterostructure. *ACS Appl. Mater. Interfaces* **6**, 22351–22358. https://doi.org/10.1021/am506336w (2014).
30. Pavlenko, N. & Kopp, T. Structural relaxation and metal-insulator transition at the interface between $SrTiO_3$ and $LaAlO_3$. *Surf. Sci.* **605**, 1114–1121. https://doi.org/10.1016/j.susc.2011.03.016 (2011).
31. Behtash, M., Nazir, S., Wang, Y. & Yang, K. Polarization effects on the interfacial conductivity in $LaAlO_3/SrTiO_3$ heterostructures: A first-principles study. *Phys. Chem. Chem. Phys.* **18**, 6831–6838. https://doi.org/10.1039/C5CP07581E (2016).
32. Li, B., Liu, Q., Zhang, Y., Liu, Z. & Geng, L. Highly conductive Nb doped $BaSnO_3$ thin films on MgO substrates by pulsed laser deposition. *J. Alloys Compd.* **680**, 343–349. https://doi.org/10.1016/j.jallcom.2016.04.157 (2016).
33. Liu, X., Wang, Y., Lukashev, P. V., Burton, J. D. & Tsymbal, E. Y. Interface dipole effect on thin film ferroelectric stability: First-principles and phenomenological modeling. *Phys. Rev. B* **85**, 125407. https://doi.org/10.1103/PhysRevB.85.125407 (2012).
34. Zhong, W., King-Smith, R. & Vanderbilt, D. Giant LO-TO splittings in perovskite ferroelectrics. *Phys. Rev. Lett.* **72**, 3618. https://doi.org/10.1103/PhysRevLett.72.3618 (1994).
35. Miglio, A. *et al.* Computed electronic and optical properties of SnO_2 under compressive stress. *Opt. Mater.* **38**, 161–166. https://doi.org/10.1016/j.optmat.2014.10.017 (2014).
36. Aggoune, W. *et al.* A consistent picture of excitations in cubic $BaSnO_3$ revealed by combining theory and experiment. *Commun. Mater.*https://doi.org/10.1038/s43246-022-00234-6 *(2021).*
37. Yu, P. Y. *Fundamentals of Semiconductors : Physics and Materials Properties* Vol. 198 (Springer, 1996).
38. Karamargin, M., Reynolds, C., Lipschultz, F. & Klemens, P. Lattice thermal conductivity and deviations from Matthiessen's rule for dilute alloys of tin with cadmium. *Phys. Rev. B* **6**, 3624. https://doi.org/10.1103/PhysRevB.6.3624 (1972).
39. Madsen, G. K. Automated search for new thermoelectric materials: The case of LiZnSb. *J. Am. Chem. Soc.* **128**, 12140–12146. https://doi.org/10.1021/ja062526a (2006).
40. Chen, W. *et al.* Understanding thermoelectric properties from high-throughput calculations: Trends, insights, and comparisons with experiment. *J. Mater. Chem. C* **4**, 4414–4426. https://doi.org/10.1039/c5tc04339e (2016).
41. Kohn, W. & Sham, L. J. Self-consistent equations including exchange and correlation effects. *Phys. Rev.* **140**, A1133. https://doi.org/10.1103/PhysRev.140.A1133 (1965).
42. Kresse, G. & Furthmüller, J. Efficient iterative schemes for ab initio total-energy calculations using a plane-wave basis set. *Phys. Rev. B* **54**, 11169. https://doi.org/10.1103/PhysRevB.54.11169 (1996).
43. Kresse, G. & Joubert, D. From ultrasoft pseudopotentials to the projector augmented-wave method. *Phys. Rev. B* **59**, 1758. https://doi.org/10.1103/PhysRevB.59.1758 (1999).
44. Blöchl, P. E. Projector augmented-wave method. *Phys. Rev. Lett.* **50**, 17953. https://doi.org/10.1103/PhysRevB.50.17953 (1994).
45. Perdew, J. P., Burke, K. & Ernzerhof, M. Generalized gradient approximation made simple. *Phys. Rev. Lett.* **77**, 3865. https://doi.org/10.1103/PhysRevLett.77.3865 (1996).
46. Monkhorst, H. J. & Pack, J. D. Special points for Brillouin-zone integrations. *Phys. Rev. B* **13**, 5188. https://doi.org/10.1103/PhysRevB.13.5188 (1976).
47. Xingyi, T., Yanjun, G., Changle, C. & Kexin, J. First-principles calculations of electronic structure and optical properties of n-type doped $BaSnO_3$. *Rare Metal Mater. Eng.* **43**, 1387–1391. https://doi.org/10.7498/aps.61.237107 (2014).

Acknowledgements

This work was supported by the National Natural Science Foundation of China (Grant No. 51802268 and 51972276). Al the numerical computations were performed on Hefei advanced computing center.

Author contributions

Y.Q.W. designed the study. Y.L.L. and Y.X.H. performed the calculations. Y. L.L., X.H.L. and L.Y. prepared figures and wrote the manuscript. All authors contributed to the interpretation of the results and the review of the manuscript.

Competing interests

The authors declare no competing interests.

Additional information

Supplementary Information The online version contains supplementary material available at https://doi.org/10.1038/s41598-024-60893-y.

Correspondence and requests for materials should be addressed to Y.W.

Reprints and permissions information is available at www.nature.com/reprints.

Publisher's note Springer Nature remains neutral with regard to jurisdictional claims in published maps and institutional affiliations.